Supplementary information accompanying "Nitrogen isotopic fractionations during nitric oxide production in an agricultural soil" by Yu and Elliott.

Table of contents

S1. Mass-dependent isotopic fractionation and $\Delta^{17}O$-NO_3^- as a conservative tracer of biogeochemical NO_3^- transformations.

The use of $\Delta^{17}O$-NO_3^- to simulate biogeochemical NO_3^- transformations hinges on the conservative nature of $\Delta^{17}O$ during mass-dependent oxygen (O) isotopic fractionations. Given the three stable O isotopes (i.e., ^{16}O, ^{17}O, and ^{18}O), fractionation of $^{17}O/^{16}O$ (^{17}R) relative to $^{18}O/^{16}O$ (^{18}R) in a normal O isotope fractionation process is proportional to the mass difference between the respective O isotopologues. Thus, for both kinetic and equilibrium fractionations of the three O isotopes, the isotopic fractionation factors for ^{17}R ($^{17}\alpha$) and ^{18}R ($^{18}\alpha$) are related by the mass-dependent fractionation law:

$$^{17}\alpha = (^{18}\alpha)^\beta \qquad\qquad \text{Equation (S1)}$$

where β is the three-isotope exponent determined exclusively by the masses of the respective O isotopologues involved in the reaction. Importantly, β is not equal to a single value but varies generally between 0.51 and 0.53 for different O isotopic fractionation processes (Miller, 2002; Young et al., 2002). Mass-dependent fractionations of the three O isotopes can be represented by a single curve on the O three-isotope plot, in which isotope ratios (^{17}R and ^{18}R) are expressed as fractional differences from a reference material ($^{17}R_{ref}$ and $^{18}R_{ref}$) lying on the same curve (i.e., Vienna Standard Mean Ocean Water (VSMOW) in this study) (Miller, 2002):

$$^{17}R/^{17}R_{ref} = (^{18}R/^{18}R_{ref})^\beta \qquad\qquad \text{Equation (S2)}$$

Taking delta notation (δ=[(R/R_{ref})-1]×1000, in units of ‰) and natural log transformation yields:

$$\ln(\delta^{17}O/1000+1) = \beta*\ln(\delta^{18}O/1000+1) \qquad\qquad \text{Equation (S3)}$$

Thus, a plot of $\ln(\delta^{17}O/1000+1)$ against $\ln(\delta^{18}O/1000+1)$ produce a straight line with a slope equal to β in the O three-isotope space, representing the mass-dependent fractionation law. On this basis, anomalous ^{17}O excess or deficiency ($\Delta^{17}O$), characterized by the departure from the mass-dependent fractionation line as a result of mass-independent isotope effects (e.g., photochemical ozone formation), is defined in delta notation as:

$$\Delta^{17}O = [\ln(\delta^{17}O/1000+1) - \beta*\ln(\delta^{18}O/1000+1)]*1000 \qquad\qquad \text{Equation (S4)}$$

Because nonzero $\Delta^{17}O$-NO_3^- values is strictly a result of photochemical effects, biogeochemical NO_3^- consumption processes in soils, such as denitrification and NO_3^- assimilation, obey the mass-dependent fractionation law (i.e., Equation (S1)), leaving $\Delta^{17}O$-NO_3^- nearly unaltered. On the other hand, the $\Delta^{17}O$-NO_3^- signal can be diluted by nitrification-produced NO_3^-, which has $\Delta^{17}O \approx 0$. The conservative behavior of $\Delta^{17}O$-NO_3^- during soil NO_3^- transformations were thoroughly examined by our previous study using soil samples spanning a wide range of nitrification and denitrification potentials (Yu and Elliott, 2018). These soil samples were amended with a Chilean NO_3^- fertilizer enriched in $\Delta^{17}O$ and subsequently monitored for variations in $\delta^{15}N$, $\delta^{18}O$, and $\Delta^{17}O$ of soil NO_3^- under controlled laboratory conditions. An isotopologue-specific (i.e., ^{14}N, ^{15}N, ^{16}O, ^{17}O, and ^{18}O) model was developed to simulate mass-dependent isotopic fractionations during co-occurring soil nitrification and NO_3^- consumption and used to inversely optimize gross rates and N isotope effects of these two processes. Results from a model sensitivity analysis showed that the optimized gross rates and N isotope effects were not sensitive to the value of β (0.51 to 0.53) and the mass-dependent O isotopic fractionations during NO_3^- production and consumption (Yu and Elliott, 2018), corroborating the conservative nature of $\Delta^{17}O$-NO_3^-. Thus, although $\delta^{18}O$ and $\delta^{17}O$ of NO_3^- are controlled by the O isotopic fractionations and their respective β values during nitrification and NO_3^- consumption, no precise knowledge of these controlling factors need be known in order to apply $\Delta^{17}O$-NO_3^- in the isotopologue-specific model. Furthermore, these results also confirmed that setting β to 0.52 for all the relevant O isotope-fractionating processes involved in nitrification and denitrification (e.g., O incorporation during nitrification, O exchange between H_2O and NO_2^-, dissimilatory NO_3^- reduction, etc.) is sufficient for simulating their impacts on $\delta^{18}O$-NO_3^- and $\Delta^{17}O$-NO_3^- (Yu and Elliott, 2018). Thus, Equation (S4) can be simplified to:

$$\Delta^{17}O = [\ln(\delta^{17}O/1000+1) - 0.52*\ln(\delta^{18}O/1000+1)]*1000 \qquad \text{Equation (S5)}$$

In summary, $\Delta^{17}O$-NO_3^- is a conservative tracer of biogeochemical NO_3^- production and consumption within the conceptual domain of mass-dependent isotopic fractionations, functioning essentially as the labeled $^{15}NO_3^-$ tracers within the domain of isotope mass balance.

S2. Control tests on the robustness of soil extraction and incubation procedures.

Two control tests were conducted to evaluate the robustness of the adopted soil extraction and incubation methods. In the first test, eight incubators containing 100 g (dry weight equivalent) soil were prepared following the protocol detailed in the main text and incubated under anoxic conditions for 6 days. Following the incubation, half of the incubators were opened from the top, and a solution of an off-the-shelf KNO_2 and the Chilean NO_3^- ($\delta^{15}N$=0.3‰, $\delta^{18}O$=55.8‰, $\Delta^{17}O$=18.6‰) was added to the soil surface using a pipette. The fertilization rate was 3 µg NO_2^--N·g^{-1} and 15 µg NO_3^--N·g^{-1}. The spiked and non-spiked samples were then extracted for NO_3^- and NO_2^- using the method described in the main text. For each sample, the resultant soil extract was split into two subsamples: one treated with sulfamic acid for NO_3^- analysis and the other without sulfamic acid treatment for analysis of NO_2^-+NO_3^-. A comparison between the results from the spiked and non-spiked samples showed that the spiked NO_2^- and NO_3^- were 100% recovered and that $\delta^{15}N$, $\delta^{18}O$, and $\Delta^{17}O$ values of the spiked Chilean NO_3^- were accurately determined after the NO_2^- removal (Table S1).

In the second test, eight incubators containing 100 g (dry weight equivalent) soil were prepared following the protocol detailed in the main text. Four of the samples were incubated following the established procedures for 3 days. The other four samples were incubated statistically under anoxic conditions by closing the vacuum valves. For each of these samples, an aliquot of concentrated acetylene (C_2H_2) (balanced by N_2) was added to the incubator headspace through the septa to achieve a headspace concentration of 10 Pascal. These samples were then incubated statistically for 3 days. Subsequent concentration and isotope analyses showed no statistical difference (Welch's t-test, $P<0.05$) between samples with and without the C_2H_2 treatment (Table S2). Because C_2H_2 at 10 Pascal blocks activities of ammonia monooxygenase in both ammonia-oxidizing bacteria and archaea (Taylor et al., 2015), these results suggest that aerobic NH_4^+ oxidation was negligible during the anoxic incubations. Collectively, these results confirmed that our water extraction method was robust for extracting soil NO_3^- and NO_2^- and that aerobic NO_3^- production during the anoxic incubation and the water extraction can be safely ruled out as an explanation for the observed declines in $\delta^{18}O$-NO_3^- and $\Delta^{17}O$-NO_3^-.

Table S1. Control test on the soil extraction method.

	NO_2^- ($\mu g\ N \cdot g^{-1}$)	NO_3^- ($\mu g\ N \cdot g^{-1}$)	$\delta^{15}N\text{-}NO_3^-$ (‰)	$\delta^{18}O\text{-}NO_3^-$ (‰)	$\Delta^{17}O\text{-}NO_3^-$ (‰)
Control (n=4)	5.5±0.1	34.0±0.3	23.8±0.5	27.4±0.2	2.2±0.2
Spiked (n=4)	8.5±0.2	49.2±0.5	16.9±0.3	35.9±0.3	7.4±0.4
Recovery	3.0±0.2[a]	15.2±0.6[a]	1.6±1.6[b]	54.9±1.4[b]	19.1±1.7[b]

a: calculated by difference between the control (i.e., non-spiked) and spiked samples. Recovery of NO_2^- and NO_3^- concentrations was 101.2±1.1% and 100.4±3.7%, respectively.

b: calculated based on an isotope mass balance of the control (i.e., non-spiked) and spiked samples. The recovered $\delta^{15}N$, $\delta^{18}O$, and $\Delta^{17}O$ values of the Chilean NO_3^- were within 1.3‰ of the true values.

Table S2. Control test on the soil incubation method.

	NO_2^- ($\mu g\ N \cdot g^{-1}$)	NO_3^- ($\mu g\ N \cdot g^{-1}$)	$\delta^{15}N\text{-}NO_3^-$ (‰)	$\delta^{18}O\text{-}NO_3^-$ (‰)	$\Delta^{17}O\text{-}NO_3^-$ (‰)
Without C_2H_2 (n=4)	0.7±0.1	40.1±0.5	11.3±0.4	31.2±0.3	6.5±0.3
With C_2H_2 (n=4)	0.9±0.0	38.9±0.7	12.1±0.3	30.5±0.4	6.1±0.2

S3. Derivation, formulation, and optimization of the isotopologue-specific model for simulating co-occurring denitrification and nitrite re-oxidation during the anoxic incubation.

S3.1. Model structure

The isotopologue-specific model simulates dynamics of ^{14}N, ^{15}N, ^{16}O, ^{17}O, and ^{18}O concentrations in soil NO_3^- and NO_2^- during co-occurring denitrification and NO_2^- re-oxidation. In order to be compatible with isotopologue calculations, the model was formulated based on isotopologue-specific process rates and net isotopic fractionation factors (α), which is related to net isotope effects (η) by: $\alpha = \eta/1000 + 1$. In the model, the reversibility of NXR was evaluated through mass and isotope balance calculations. To first order, we assumed that the forward (NXR-catalyzed NO_3^- reduction) and backward (NXR-catalyzed NO_2^- oxidation) reactions are balanced in terms of mass (i.e., no net oxidation or reduction) and that both the forward and backward reactions follow first order kinetics. Consequently, the forward reaction is related to the backward reaction following Equation (S6):

$$k_{NXR(f)}*[NO_3^-] = k_{NXR(b)}*[NO_2^-] \qquad \text{Equation (S6)}$$

where $k_{NXR(f)}$ and $k_{NXR(b)}$ are the first-order rate constants of the forward reaction and backward reactions, respectively. Furthermore, the equilibrium fractionation factor for the NXR-catalyzed NO_3^-/NO_2^- interconversion ($^{15}\alpha_{NXR(eq)}$) is related to the kinetic fractionation factors for the forward ($^{15}\alpha_{k,NXR(f)}$) and back ($^{15}\alpha_{k,NXR(b)}$) reactions (Fry, 2006):

$$^{15}\alpha_{NXR(eq)} = {}^{15}\alpha_{k,NXR(b)}/{}^{15}\alpha_{k,NXR(f)} \qquad \text{Equation (S7)}$$

Therefore, based on Equations (S6) and (S7), the NXR-driven isotope exchange between NO_3^- and NO_2^- is realized through two kinetic processes of opposite directions in the model.

To simulate the observed variations in $\delta^{18}O$ and $\Delta^{17}O$ of soil NO_3^-, two model scenarios were designed with respect to oxygen (O) isotope exchange between H_2O and NO_2^-. In the "no exchange" scenario, the model simulates ^{16}O, ^{17}O, and ^{18}O concentrations of both NO_3^- and NO_2^- pools by explicitly considering O isotopic fractionations associated with denitrifier-catalyzed NO_3^- reduction ($^{17/18}\alpha_{NAR}$), NXR-catalyzed NO_3^- reduction ($^{17/18}\alpha_{k,NXR(f)}$), abstraction of one O atom during NO_3^- reduction to NO_2^- ($^{17/18}\alpha_{NAR(br)}$), NXR-catalyzed NO_2^- oxidation ($^{17/18}\alpha_{k,NXR(b)}$), H_2O incorporation during NXR-catalyzed

NO_2^- oxidation ($^{17/18}\alpha_{NXR(H2O)}$), NIR-catalyzed NO_2^- reduction ($^{17/18}\alpha_{NIR}$), and abiotic NO_2^- reduction ($^{17/18}\alpha_{NO2/NO(abiotic)}$) (Fig. S1). In the "complete exchange" scenario, the standing NO_2^- pool is always in equilibrium with soil H_2O ($\delta^{18}O$-$H_2O\approx-10‰$, $\Delta^{17}O$-$H_2O=0‰$) in terms of O isotopes (Fig. S1). Accordingly, the model does not explicitly track dynamics of NO_2^- O isotopologues, but in instead calculates a set of equilibrium values for the fractional abundances of ^{16}O, ^{17}O, and ^{18}O in NO_2^- ($^{16}F_{NO2(eq)}$, $^{17}F_{NO2(eq)}$, $^{18}F_{NO2(eq)}$) using the equilibrium fractionation factor for O exchange between NO_2^- and H_2O ($^{17/18}\alpha_{H2O/NO2(eq)}$). To drive the model, the fractionation factors for ^{18}O relative to ^{16}O ($^{18}\alpha$) were either set to literature values derived in pure culture studies (i.e., $^{18}\alpha_{NAR(br)}$, $^{18}\alpha_{k,NXR(b)}$, $^{18}\alpha_{NXR(H2O)}$) (summarized by Granger and Wankel (2016)) or assumed to be coupled to their counterparts for fractionation of ^{15}N relative to ^{14}N (i.e., $^{18}\alpha_{NAR}$, $^{18}\alpha_{k,NXR(f)}$, $^{18}\alpha_{NIR}$, $^{18}\alpha_{NO2/NO(abiotic)}$) (Table S3). For fractionations of ^{17}O relative to ^{16}O, the fractionation factors ($^{17}\alpha$) were estimated from $^{18}\alpha$ and the mass-dependent fractionation law (Equation (S1)) using a constant β value of 0.52. Importantly, although simulations of $\delta^{18}O$-NO_3^- and $\delta^{18}O$-NO_2^- in the model are highly sensitive to the absolute magnitude of the individual O isotopic fractionations mentioned above, simulations of $\Delta^{17}O$-NO_3^- and $\Delta^{17}O$-NO_2^- are quantitative and not affected by the lack of constraints on the O isotopic fractionation factors. This is because $\Delta^{17}O$ is calculated based on the mass-dependent fractionation law and thereby only sensitive to variations in the relative abundances of ^{17}O and ^{18}O in NO_3^- and NO_2^- (Yu and Elliott, 2018). Equations used in the isotopologue-specific model for the "no exchange" and "complete exchange" scenarios are given in Box S1 and Box S2, respectively. Description of relevant parameters is provided in Table S3.

The first step in using the isotopologue-specific model to estimate process rates and isotope effects was to calculate the concentrations of ^{15}N and ^{14}N in NO_3^- and NO_2^- and the concentrations of ^{16}O, ^{17}O, and ^{18}O in NO_3^- for each sample using the isotope ratio and concentration measurements. To solve the isotoplogue-specific differential system of equations, initial isotopologue concentrations of NO_3^- and NO_2^- are required. While the initial concentrations of ^{14}N, ^{15}N, ^{16}O, ^{17}O, and ^{18}O in NO_3^- are available from the direct measurements, the initial $^{15}N/^{14}N$, $^{17}O/^{16}O$, and $^{18}O/^{16}O$ ratios of NO_2^- were not measured due to the low NO_2^- concentration at the first sampling event. Therefore, for both model scenarios, the

initial $\delta^{15}N\text{-}NO_2^-$ value ($\delta^{15}N\text{-}NO_2^-_{(t0)}$) was approximated using the initial $\delta^{15}N\text{-}NO_3^-$ value ($\delta^{15}N\text{-}NO_3^-_{(t0)}$) and the prescribed $^{15}\eta_{NAR}$: $\delta^{15}N\text{-}NO_2^-_{(t0)} = \delta^{15}N\text{-}NO_3^-_{(t0)} - {}^{15}\eta_{NAR}$. For the "no exchange" scenario, the initial $\delta^{18}O$ and $\Delta^{17}O$ values of NO_2^- were set to those of NO_3^-. Results from a sensitivity analysis confirmed that uncertainties in the initial isotopic composition of NO_2^- did not qualitatively change the optimization results, probably because of the small initial isotopologue pool sizes of NO_2^-, which could be quickly changed by subsequent NO_2^- production and consumption during the anoxic incubation. With the supplied initial conditions, the isotopologue-specific model was solved numerically using a Runge-Kutta method with a 0.5 h time step (Solver ode45, Matlab, Mathworks, USA). The obtained isotopologue abundances were then resembled to bulk concentrations and delta values ($\delta^{15}N$, $\delta^{18}O$, and $\Delta^{17}O$) of NO_3^- and NO_2^- for interpretation.

Next, the net NO production rate ($f_{NO\text{-}anoxic}$) and $\delta^{15}N\text{-}NO$ were modeled from the numerically solved NO_2^- concentration and $\delta^{15}N\text{-}NO_2^-$ values. Specifically, the net NO production were modeled from both abiotic NO_2^- reduction ($f_{abiotic}$) and coupled NO production by NIR and reduction by NOR (f_{dnf}) (Fig. S1):

$$f_{NO\text{-}anoxic} = f_{abiotic} + f_{dnf} = s_{abiotic} * k_{NO2/NO(abiotic)} * [NO_2^-] + (R_{NIR} - R_{NOR}) \qquad \text{Equation (S8)}$$

where $k_{abiotic}$ is the pseudo-first order rate constant for NO_2^- loss; $s_{abiotic}$ is the apparent stoichiometric coefficient for NO production from NO_2^-; R_{NIR} and R_{NOR} are the zero-order rate constants of NIR-catalyzed NO_2^- reduction and NOR-catalyzed NO reduction, respectively (Table S3). The $\delta^{15}N$ of abiotically produced NO ($\delta^{15}N\text{-}NO_{(abiotic)}$) was modeled using the numerically solved $\delta^{15}N\text{-}NO_2^-$ and the N isotope effect for NO production from abiotic NO_2^- reduction ($^{15}\eta_{NO2/NO(abiotic)}$) quantified in the abiotic incubation: $\delta^{15}N\text{-}NO_{(abiotic)} = \delta^{15}N\text{-}NO_2^- - {}^{15}\eta_{NO2/NO(abiotic)}$. The $\delta^{15}N$ of net NO production from the coupled NO production and reduction in denitrification ($\delta^{15}N\text{-}NO_{(dnf)}$) was modeled using the closed-system Rayleigh equation:

$$\delta^{15}N\text{-}NO_{(dnf)} = (\delta^{15}N\text{-}NO_2^- - {}^{15}\eta_{NIR}) - Ln(1 - R_{NOR}/R_{NIR}) * {}^{15}\eta_{NOR} \qquad \text{Equation (S9)}$$

where $^{15}\eta_{NIR}$ and $^{15}\eta_{NOR}$ are the N isotope effects for NIR-catalyzed NO_2^- reduction and NOR-catalyzed NO reduction, respectively. The closed-system model, rather than the open-system one, was used here to

account for the inherently non-steady state nature of N transformations in the heterogeneous soil environment (Lewicka-Szcebak et al., 2014). Based on the simulated δ^{15}N-NO$_{(abiotic)}$ and δ^{15}N-NO$_{(dnf)}$, δ^{15}N of the total net NO production was calculated using a two-source mixing model:

$$\delta^{15}\text{N-NO} = (f_{abiotic} * \delta^{15}\text{N-NO}_{(abiotic)} + f_{dnf} * \delta^{15}\text{N-NO}_{(dnf)})/(f_{abiotic} + f_{dnf}) \qquad \text{Equation (S10)}$$

S3.2. Model optimization

A nonlinear optimization applying Trust-Region-Reflective least squares algorithm (Matlab, Mathworks, USA) was used to find the unknown N process rates and N isotope effects in the isotopologue-specific model by minimizing the error-weighted residual sum of squares (RSS) between the simulated and measured results:

$$RSS = \sum_{i=1}^{n} \sum_{j=1}^{8} \frac{(S_{ij} - M_{ij})^2}{\sigma_{ij}^2} \qquad \text{Equation (S11)}$$

where n is the number of variables, S_{ij} and M_{ij} are the simulated and measured variable i at the j-th sampling event, σ_{ij} is the standard deviation between replicates. During the first modeling stage, R_{NAR}, R_{NIR}, R_{NOR}, and $k_{NXR(b)}$ were inversely optimized for each of the two model scenarios through minimizing the error-weighted RSS between the simulated and measured NO$_3^-$ and NO$_2^-$ concentrations, $f_{NO-anoxic}$, Δ^{17}O-NO$_3^-$. During the second modeling stage, an enumeration approach was used to obtain the best combination of $^{15}\eta_{NAR}$, $^{15}\eta_{NXR(eq)}$, $^{15}\eta_{NIR}$, and $^{15}\eta_{NOR}$ that minimizes the error-weighted RSS between the simulated and measured δ^{15}N values of NO$_3^-$, NO$_2^-$, and NO. Due to the high nonlinearity of the modeling system, the inverse optimization procedure was repeated 100 times with different initial guesses for variables to be optimized to avoid local minima. Approximate 95% confidence intervals were calculated for variable estimates using an error covariance matrix (Yu and Elliott, 2018).
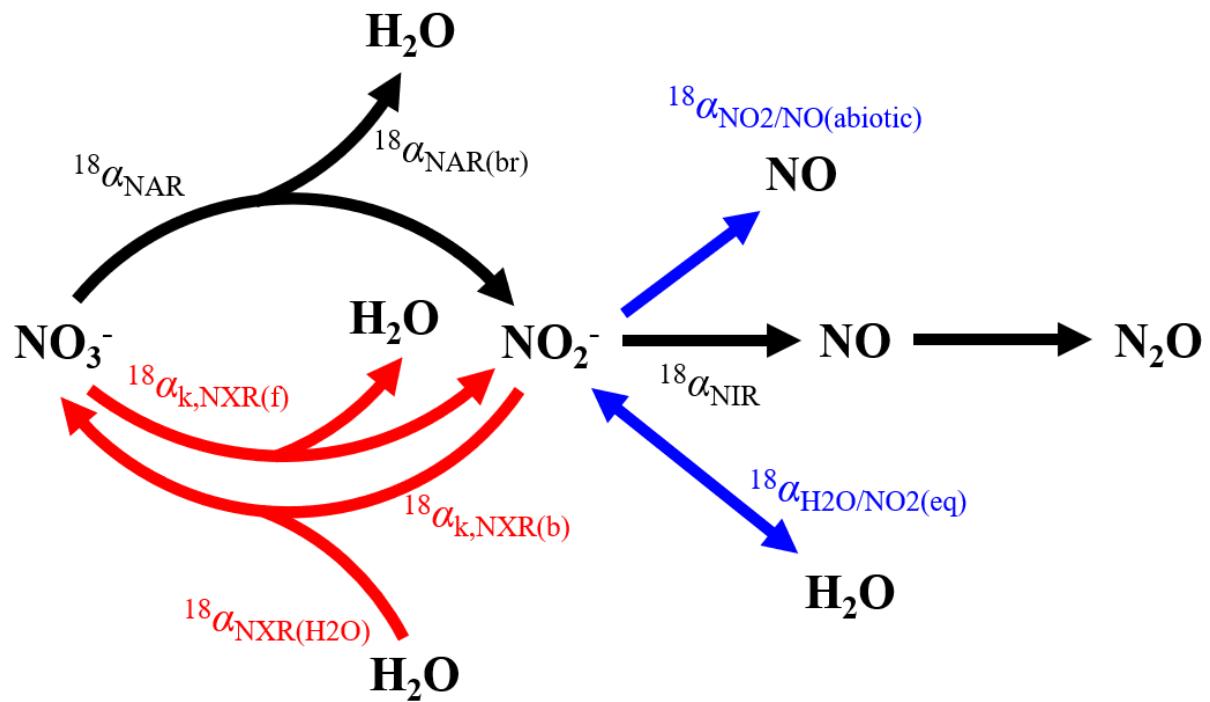
Figure S1. Model structure of co-occurring denitrification and NO_2^- re-oxidation and associated O isotopic fractionations. Values of the O isotopic fractionation factors are given in Table S3.

Box S1. Equations used in the isotopologue-specific model for simulating co-occurring denitrification and nitrite re-oxidation under the "no exchange" model scenario.

$$d[^{14}N]_{NO3}/dt = k_{NXR(b)}*[^{14}N]_{NO2} - k_{NXR(f)}*[^{14}N]_{NO3} - R_{NAR}*^{14}F_{NO3}$$

$$d[^{15}N]_{NO3}/dt = k_{NXR(b)}/^{15}\alpha_{k,NXR(b)}*[^{15}N]_{NO2} - k_{NXR(f)}/^{15}\alpha_{k,NXR(f)}*[^{15}N]_{NO3} - R_{NAR}/^{15}\alpha_{NAR}*^{15}F_{NO3}$$

$$d[^{14}N]_{NO2}/dt = R_{NAR}*^{14}F_{NO3} + k_{NXR(f)}*[^{14}N]_{NO3} - R_{NIR}*^{14}F_{NO2} - k_{NXR(b)}*[^{14}N]_{NO2} - k_{abiotic}*[^{14}N]_{NO2}$$

$$d[^{15}N]_{NO2}/dt = R_{NAR}/^{15}\alpha_{NAR}*^{15}F_{NO3} + k_{NXR(f)}/^{15}\alpha_{k,NXR(f)}*[^{15}N]_{NO3} - R_{NIR}/^{15}\alpha_{NIR} \; *^{15}F_{NO2}$$
$$- k_{NXR(b)}/^{15}\alpha_{k,NXR(b)}*[^{15}N]_{NO2} - k_{abiotic}/^{15}\alpha_{NO2/NO(abiotic)}*[^{14}N]_{NO2}$$

$$d[^{16}O]_{NO3}/dt = k_{NXR(b)}*([^{16}O]_{NO2} + [^{14}N]_{NO2}*^{16}F_{H2O}) - k_{NXR(f)}*[^{16}O]_{NO3} - 3*R_{NAR}*^{16}F_{NO3}$$

$$d[^{17}O]_{NO3}/dt = k_{NXR(b)}*([^{17}O]_{NO2}/(^{18}\alpha_{k,NXR(b)})^{0.52} + [^{14}N]_{NO2}*^{17}F_{H2O}/(^{18}\alpha_{NXR(H2O)})^{0.52})$$
$$- k_{NXR(f)}/(^{18}\alpha_{k,NXR(f)})^{0.52}*[^{17}O]_{NO3} - 3*R_{NAR}/(^{18}\alpha_{NAR})^{0.52}*^{17}F_{NO3}$$

$$d[^{18}O]_{NO3}/dt = k_{NXR(b)}*([^{18}O]_{NO2}/^{18}\alpha_{k,NXR(b)} + [^{14}N]_{NO2}*^{18}F_{H2O}/^{18}\alpha_{NXR(H2O)}) - k_{NXR(f)}/^{18}\alpha_{k,NXR(f)}*[^{18}O]_{NO3}$$
$$- 3*R_{NAR}/^{18}\alpha_{NAR}*^{18}F_{NO3}$$

$$d[^{16}O]_{NO2}/dt = 2/3*3*R_{NAR}*^{16}F_{NO3} + 2/3*k_{NXR(f)}*[^{16}O]_{NO3} - 2*R_{NIR}*^{16}F_{NO2} - k_{NXR(b)}*[^{16}O]_{NO2}$$
$$- k_{abiotic}*[^{16}O]_{NO2}$$

$$d[^{17}O]_{NO2}/dt = 2/3*3*R_{NAR}/(^{18}\alpha_{NAR})^{0.52}/(^{18}\alpha_{NAR(br)})^{0.52}*^{17}F_{NO3}$$
$$+ 2/3*k_{NXR(f)}/(^{18}\alpha_{k,NXR(f)})^{0.52}/(^{18}\alpha_{NAR(br)})^{0.52}*[^{17}O]_{NO3} - 2*R_{NIR}/(^{18}\alpha_{NIR})^{0.52}*^{17}F_{NO2}$$
$$- k_{NXR(b)}/(^{18}\alpha_{k,NXR(b)})^{0.52}*[^{17}O]_{NO2} - k_{abiotic}/(^{18}\alpha_{NO2/NO(abiotic)})^{0.52}*[^{17}O]_{NO2}$$

$$d[^{18}O]_{NO2}/dt = 2/3*3*R_{NAR}/^{18}\alpha_{NAR}/^{18}\alpha_{NAR(br)}*^{18}F_{NO3} + 2/3*k_{NXR(f)}/^{18}\alpha_{k,NXR(f)}/^{18}\alpha_{NAR(br)}*[^{18}O]_{NO3}$$
$$- 2*R_{NIR}/^{18}\alpha_{NIR}*^{18}F_{NO2} - k_{NXR(b)}/^{18}\alpha_{k,NXR(b)}*[^{18}O]_{NO2} - k_{abiotic}/^{18}\alpha_{NO2/NO(abiotic)}*[^{18}O]_{NO2}$$

Box S2. Equations used in the isotopologue-specific model for simulating co-occurring denitrification and nitrite re-oxidation under the "complete exchange" model scenario.

$$d[^{14}N]_{NO3}/dt = k_{NXR(b)}*[^{14}N]_{NO2} - k_{NXR(f)}*[^{14}N]_{NO3} - R_{NAR}*^{14}F_{NO3}$$

$$d[^{15}N]_{NO3}/dt = k_{NXR(b)}/^{15}\alpha_{k,NXR(b)}*[^{15}N]_{NO2} - k_{NXR(f)}/^{15}\alpha_{k,NXR(f)}*[^{15}N]_{NO3} - R_{NAR}/^{15}\alpha_{NAR}*^{15}F_{NO3}$$

$$d[^{14}N]_{NO2}/dt = R_{NAR}*^{14}F_{NO3} + k_{NXR(f)}*[^{14}N]_{NO3} - R_{NIR}*^{14}F_{NO2} - k_{NXR(b)}*[^{14}N]_{NO2} - k_{abiotic}*[^{14}N]_{NO2}$$

$$d[^{15}N]_{NO2}/dt = R_{NAR}/^{15}\alpha_{NAR}*^{15}F_{NO3} + k_{NXR(f)}/^{15}\alpha_{k,NXR(f)}*[^{15}N]_{NO3} - R_{NIR}/^{15}\alpha_{NIR}*^{15}F_{NO2}$$
$$- k_{NXR(b)}/^{15}\alpha_{k,NXR(b)}*[^{15}N]_{NO2} - k_{abiotic}/^{15}\alpha_{NO2/NO(abiotic)}*[^{14}N]_{NO2}$$

$$d[^{16}O]_{NO3}/dt = k_{NXR(b)}*[^{14}N]_{NO2}*(2*^{16}F_{NO2(eq)} + {}^{16}F_{H2O}) - k_{NXR(f)}*[^{16}O]_{NO3} - 3*R_{NAR}*^{16}F_{NO3}$$

$$d[^{17}O]_{NO3}/dt = k_{NXR(b)}*[^{14}N]_{NO2}*(2*^{17}F_{NO2(eq)}/(^{18}\alpha_{k,NXR(b)})^{0.52} + {}^{17}F_{H2O}/(^{18}\alpha_{NXR(H2O)})^{0.52})$$
$$- k_{NXR(f)}/(^{18}\alpha_{k,NXR(f)})^{0.52}*[^{17}O]_{NO3} - 3*R_{NAR}/(^{18}\alpha_{NAR})^{0.52}*^{17}F_{NO3}$$

$$d[^{18}O]_{NO3}/dt = k_{NXR(b)}*[^{14}N]_{NO2}*(2*^{18}F_{NO2(eq)}/^{18}\alpha_{k,NXR(b)} + {}^{18}F_{H2O}/^{18}\alpha_{NXR(H2O)}) - k_{NXR(f)}/^{18}\alpha_{k,NXR(f)}*[^{18}O]_{NO3}$$
$$- 3*R_{NAR}/^{18}\alpha_{NAR}*^{18}F_{NO3}$$

Table S3. Parameters used in the isotopologue-specific model for simulating co-occurring denitrification and nitrite re-oxidation.

Parameter	Description	Value	Comment
$[^{14}N]$, $[^{15}N]$, $[^{16}O]$, $[^{17}O]$, $[^{18}O]$	N or O isotopologue concentration		Simulated by the model
^{14}F and ^{15}F	Fractional abundance of ^{14}N and ^{15}N		Calculated from isotopologue concentrations
^{16}F, ^{17}F, and ^{18}F	Fractional abundance of ^{16}O, ^{17}O, and ^{18}O		Calculated from isotopologue concentrations
$^{16}F_{NO2(eq)}$, $^{17}F_{NO2(eq)}$, and $^{18}F_{NO2(eq)}$	Fractional abundance of ^{16}O, ^{17}O, and ^{18}O in NO_2^- at equilibrium with soil water		Calculated using $\delta^{18}O$-H_2O (-10‰), $\Delta^{17}O$-H_2O (0‰), and equilibrium isotope effect between NO_2^- and H_2O ($^{18}\eta_{H2O/NO2(eq)}$=14‰)
R_{NAR}	Zero order rate for NO_3^- reduction		Optimized by the model
R_{NIR}	Zero order rate for NO_2^- reduction		Optimized by the model
R_{NOR}	Zero order rate for NO reduction		Optimized by the model
$k_{NXR(b)}$	First order rate constant of NXR-catalyzed NO_2^- oxidation		Optimized by the model
$k_{NXR(f)}$	First order rate constant of NXR-catalyzed NO_3^- reduction		Calculated from $k_{NXR(b)}$ using Equation (S7) for each model iteration
$k_{abiotic}$	First order rate constant of abiotic NO_2^- reduction	0.0027 h^{-1}	Fixed value.
$s_{abiotic}$	Apparent stoichiometric coefficient for abiotic NO production from NO_2^-	0.52	Fixed value.
$^{15}\alpha_{NXR(eq)}$	Equilibrium fractionation factor for NXR-catalyzed NO_3^- and NO_2^- interconversion	0.940 to 1	
$^{15}\alpha_{k,NXR(b)}$	N fractionation factor for NXR-catalyzed NO_2^- oxidation		Calculated from $^{15}\alpha_{NXR(eq)}$ and $^{15}\alpha_{k,NXR(f)}$ using Equation (S6) for each model iteration.

$^{18}\alpha_{k,NXR(b)}$	O fractionation factor for NXR-catalyzed NO_2^- oxidation	0.996	Buchwald and Casciotti, (2010)
$^{18}\alpha_{NXR(H2O)}$	O fractionation factor for H_2O incorporation during NXR-catalyzed NO_2^- oxidation	1.014	Buchwald and Casciotti, (2010)
$^{15}\alpha_{k,NXR(f)}$	N fractionation factor for NXR-catalyzed NO_3^- reduction		Set to be equal to $^{15}\alpha_{NAR}$
$^{18}\alpha_{k,NXR(f)}$	O fractionation factor for NXR-catalyzed NO_3^- reduction		Set to be coupled to $^{15}\alpha_{k,NXR(f)}$
$^{15}\alpha_{NAR}$	N fractionation factor for NO_3^- reduction by denitrifiers	1.005 to 1.055	
$^{18}\alpha_{NAR}$	O fractionation factor for NO_3^- reduction by denitrifiers		Coupled to $^{15}\alpha_{NAR}$
$^{18}\alpha_{NAR(br)}$	O fractionation factor for branching O removal during NO_3^- reduction by denitrifiers	0.975	Casciotti et al., (2002). $^{18}\alpha_{NAR(br)}$ is parameterized as an inverse isotopic fractionation in the model because it acts to enrich ^{18}O in NO_2^- during NO_3^- reduction.
$^{15}\alpha_{NIR}$	N fractionation factor for NO_2^- reduction by denitrifiers		Optimized by the model for every possible combination of $^{15}\alpha_{NAR}$ and $^{15}\alpha_{NXR(eq)}$
$^{18}\alpha_{NIR}$	O fractionation factor for NO_2^- reduction by denitrifiers		Coupled to $^{15}\alpha_{NIR}$
$^{15}\alpha_{NO2/NO(abiotic)}$	N fractionation factor for abiotic NO production from NO_2^-	1.019	Fixed value.
$^{18}\alpha_{NO2/NO(abiotic)}$	O fractionation factor for abiotic NO production from NO_2^-		Coupled to $^{15}\alpha_{NO2/NO(abiotic)}$
$^{15}\alpha_{NOR}$	N fractionation factor for NO reduction by denitrifiers		Optimized by the model for every possible combination of $^{15}\alpha_{NAR}$ and $^{15}\alpha_{NXR(eq)}$

S4. Forward modeling of $\delta^{18}O$-NO_3^- under the "no exchange" and "complete exchange" scenarios.

The isotopologue-specific model with optimized rates of denitrification and NO_2^- re-oxidation was used to explore whether the observed decrease in $\delta^{18}O$-NO_3^- can be possibly explained by co-occurring denitrification and NO_2^- re-oxidation under the "no exchange" and "complete exchange" scenarios. Specifically, to simulate $\delta^{18}O$-NO_3^- variations, the model was forwarded using published O isotopic fractionation factors for the branching O isotopic fractionation during NO_3^- reduction to NO_2^- ($^{18}\eta_{NAR(br)}$), NXR-catalyzed NO_2^- oxidation ($^{18}\eta_{k,NXR(b)}$), H_2O incorporation during NXR-catalyzed NO_2^- oxidation ($^{18}\eta_{NXR(H2O)}$), and O exchange between NO_2^- and H_2O ($^{18}\eta_{H2O/NO2(eq)}$) (Fig. S1) (values of the corresponding $^{18}\alpha$ are provided in Table S3). Moreover, to examine how variations in $\delta^{18}O$-NO_3^- are regulated by O isotopic fractionations associated with NO_3^- reduction and NO_2^- re-oxidation, the forward modeling was coupled to a sensitivity analysis, in which the magnitude of O isotope effect for denitrifier-catalyzed NO_3^- reduction ($^{18}\eta_{NAR}$) was varied from 5 to 55‰. As shown in Fig. S2a, the forward modeled $\delta^{18}O$-NO_3^- was highly sensitive to the model scenarios and the prescribed value of $^{18}\eta_{NAR}$. Specifically, the observed decreasing trend in $\delta^{18}O$-NO_3^- could be well reproduced under the "complete exchange" scenario using a $^{18}\eta_{NAR} \leq 25$‰. However, under the "no exchange" scenario, the decreasing trend could not be simulated, even with a very small $^{18}\eta_{NAR}$ (5‰). This is mainly due to the preservation of "denitrification imprints" in the standing NO_2^- pool under the "no exchange" scenario. During NAR-catalyzed NO_3^- reduction, lighter O isotopes are preferentially abstracted from NO_3^- molecules, leading to enrichment of ^{18}O in the product NO_2^- (i.e., the branching O isotope effect) (Casciotti et al., 2002). Consequently, the $\delta^{18}O$ of NO_2^- being re-oxidized back to NO_3^- was also elevated, contributing to the simulated increases in $\delta^{18}O$-NO_3^- under the "no exchange" scenario (Fig. S2a). Therefore, the contrasting patterns in the forward modeled $\delta^{18}O$-NO_3^- between the two model scenarios (Fig. S2a) seem to suggest that O exchange between NO_2^- and H_2O indeed occurred to a high degree during the anoxic incubation. However, the forward modeled $\delta^{18}O$-NO_3^- variations are highly sensitive to the prescribed O isotope effects, which have only been quantified in less than a handful of pure culture studies (Granger and Wankel, 2016). For example, to our best knowledge, the branching O isotope effect for NO_3^- reduction ($^{18}\eta_{NAR(br)}$), which plays a pivotal role in regulating the

modeled $\delta^{18}O\text{-}NO_3^-$ trajectory, has so far only been reported for two strains of denitrifying bacteria

(Casciotti et al., 2002). It is entirely possible that transformations between NO_3^- and NO_2^- catalyzed by

whole denitrifier and NOB communities in this agricultural soil were associated with O isotopic

fractionations different from those reported in previous pure culture studies. If we reduced $^{18}\eta_{NAR(br)}$ from

the previously reported value of 25‰ to 15‰, the decreasing $\delta^{18}O$ trend could be successfully reproduced

under the "no exchange" scenario with a $^{18}\eta_{NAR} \leq 15$‰ (Fig. S2b). In sum, results from this forward

modeling exercise highlight the competing isotope effects between NO_3^- reduction and NO_2^- re-oxidation

and provide evidence that decreases in $\delta^{18}O\text{-}NO_3^-$ can occur when enrichment of ^{18}O in NO_3^- during NO_3^-

reduction is offset by the low $\delta^{18}O$ value of NO_3^- produced from NO_2^- re-oxidation (Fig. S2).
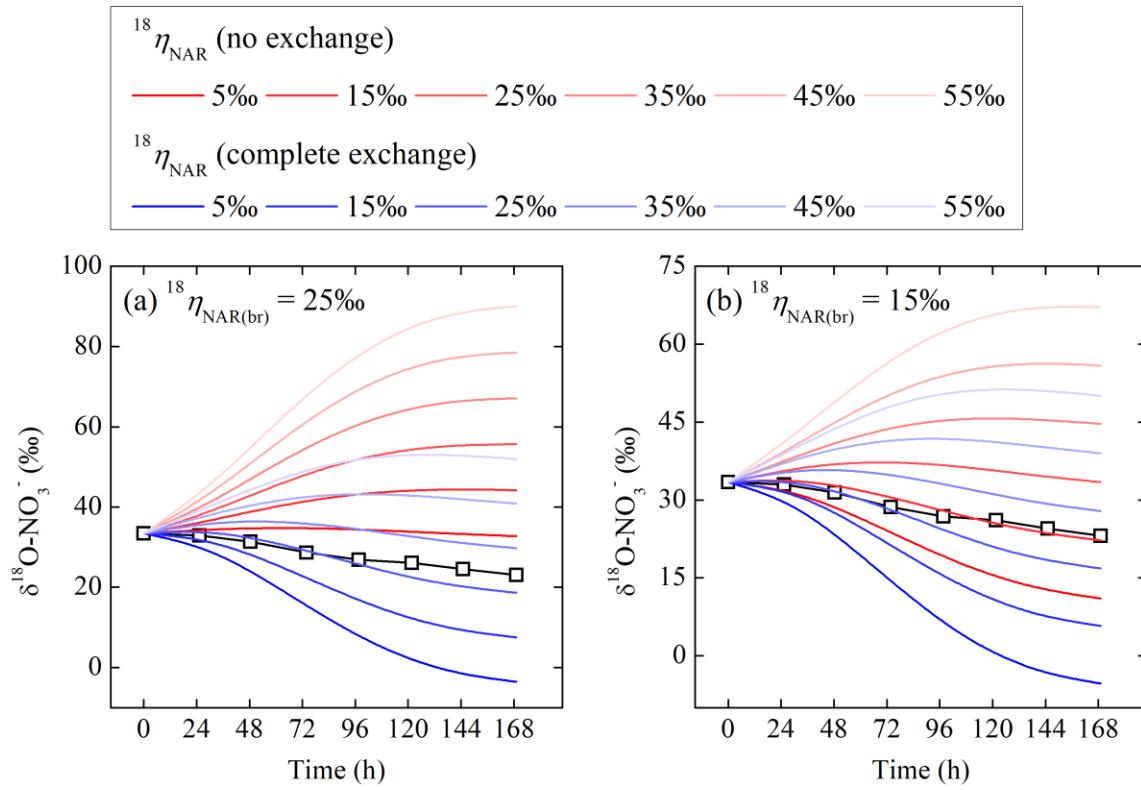
Figure S2. Forward modeled $\delta^{18}O\text{-}NO_3^-$ (lines) as a function of O isotope effect for NO_3^- reduction

($^{18}\eta_{NAR}$) under the "no exchange" and "complete exchange" scenarios. Two different values of branching

O isotope effect for NO_3^- reduction ($^{18}\eta_{NAR(br)}$) was used for the forward modeling: (a) $^{18}\eta_{NAR(br)} = 25$‰

and (b) $^{18}\eta_{NAR(br)} = 15$‰. The measured $\delta^{18}O\text{-}NO_3^-$ (line and open square) was also shown for comparison.

S5. The isotopologue-specific model for simulating net mineralization, gross nitrification, and gross NO₃⁻ consumption during the oxic and hypoxic incubation.

The isotopologue-specific model developed by Yu and Elliott (2018) was applied here to simulate net mineralization, gross nitrification, and gross NO_3^- consumption during the oxic and hypoxic incubations. Three soil N pools were considered in the model: organic N, NH_4^+, and NO_3^-. Mineralization of organic N produces NH_4^+, which can be returned to the organic N pool via microbial NH_4^+ assimilation or nitrified to NO_3^-, while NO_3^- can be consumed via microbial assimilation and denitrification. NO_2^- was not explicitly included in the model because it was not in significant concentrations in either incubation experiment. Moreover, mineralization and NH_4^+ assimilation fluxes were combined to be a net mineralization flux between the organic N and NH_4^+ pools to lower the number of unknowns in the model. Because soil organic N was not measured in this study, we assumed it could be approximated by the total soil N in terms of pool size (0.2%) and N isotopic composition (5.3‰) (Yu and Elliott, 2018). Each of three considered N transformation processes was associated with a kinetic N isotope effect. During the two-step process of nitrification, oxidation of NH_3 to NO_2^- incorporates one O atom from O_2 and one from H_2O; the subsequent oxidation of NO_2^- to NO_3^- incorporates an O atom derived from H_2O. Incorporation of each of the three O atoms was associated with a kinetic O isotope effect (Granger and Wankel, 2016). To drive the model, we used 23.5‰ and -10‰ for $\delta^{18}O$ of soil O_2 and H_2O, respectively. Assuming that concentration and $\delta^{15}N$ of organic N did not change significantly during the short-term oxic and hypoxic incubations, the gross rates and net N isotope effects of net mineralization, gross nitrification, and gross NO_3^- consumption were inversely optimized by minimizing the error-weighted residual sum of squares between the simulated and measured NH_4^+ and NO_3^- concentrations, $\delta^{15}N$ values of NH_4^+ and NO_3^-, and $\Delta^{17}O\text{-}NO_3^-$ from all three $\delta^{15}N\text{-}NH_4^+$ treatments. Formulation of the isotopologue-specific model is given in Box S3. Description of parameters used in the model is provided in Table S4.

Box S3. Equations used in the isotopologue-specific model for simulating net mineralization, nitrification, and nitrate consumption.

$$\mathrm{d}[^{14}\mathrm{N}]_{\mathrm{OrgN}}/\mathrm{dt} = -R_{\mathrm{OrgN/NH4}}*{}^{14}\mathrm{F}_{\mathrm{OrgN}}$$

$$\mathrm{d}[^{15}\mathrm{N}]_{\mathrm{OrgN}}/\mathrm{dt} = -R_{\mathrm{OrgN/NH4}}/{}^{15}\alpha_{\mathrm{OrgN/NH4}}*{}^{15}\mathrm{F}_{\mathrm{OrgN}}$$

$$\mathrm{d}[^{14}\mathrm{N}]_{\mathrm{NH4}}/\mathrm{dt} = R_{\mathrm{OrgN/NH4}}*{}^{14}\mathrm{F}_{\mathrm{OrgN}} - R_{\mathrm{NH4/NO3}}*{}^{14}\mathrm{F}_{\mathrm{NH4}}$$

$$\mathrm{d}[^{15}\mathrm{N}]_{\mathrm{NH4}}/\mathrm{dt} = R_{\mathrm{OrgN/NH4}}/{}^{15}\alpha_{\mathrm{OrgN/NH4}}*{}^{15}\mathrm{F}_{\mathrm{OrgN}} - R_{\mathrm{NH4/NO3}}/{}^{15}\alpha_{\mathrm{NH4/NO3}}*{}^{15}\mathrm{F}_{\mathrm{NH4}}$$

$$\mathrm{d}[^{14}\mathrm{N}]_{\mathrm{NO3}}/\mathrm{dt} = R_{\mathrm{NH4/NO3}}*{}^{14}\mathrm{F}_{\mathrm{NH4}} - R_{\mathrm{NO3comp}}*{}^{14}\mathrm{F}_{\mathrm{NO3}}$$

$$\mathrm{d}[^{15}\mathrm{N}]_{\mathrm{NO3}}/\mathrm{dt} = R_{\mathrm{NH4/NO3}}/{}^{15}\alpha_{\mathrm{NH4/NO3}}*{}^{15}\mathrm{F}_{\mathrm{NH4}} - R_{\mathrm{NO3comp}}/{}^{15}\alpha_{\mathrm{NO3comp}}*{}^{15}\mathrm{F}_{\mathrm{NO3}}$$

$$\mathrm{d}[^{16}\mathrm{O}]_{\mathrm{NO3}}/\mathrm{dt} = R_{\mathrm{NH4/NO3}}*({}^{16}\mathrm{F}_{\mathrm{O2}} + {}^{16}\mathrm{F}_{\mathrm{H2O}}) + R_{\mathrm{NH4/NO3}}*{}^{16}\mathrm{F}_{\mathrm{H2O}} - 3*R_{\mathrm{NO3comp}}*{}^{16}\mathrm{F}_{\mathrm{NO3}}$$

$$\mathrm{d}[^{17}\mathrm{O}]_{\mathrm{NO3}}/\mathrm{dt} = R_{\mathrm{NH4/NO3}}*({}^{17}\mathrm{F}_{\mathrm{O2}}/({}^{18}\alpha_{\mathrm{AMO(O2)}})^{0.52} + {}^{17}\mathrm{F}_{\mathrm{H2O}}/({}^{18}\alpha_{\mathrm{AMO(H2O)}})^{0.52})$$
$$+ R_{\mathrm{NH4/NO3}}*{}^{17}\mathrm{F}_{\mathrm{H2O}}/({}^{18}\alpha_{\mathrm{NXR(H2O)}})^{0.52} - 3*R_{\mathrm{NO3comp}}/({}^{18}\alpha_{\mathrm{NO3comp}})^{0.52}*{}^{17}\mathrm{F}_{\mathrm{NO3}}$$

$$\mathrm{d}[^{18}\mathrm{O}]_{\mathrm{NO3}}/\mathrm{dt} = R_{\mathrm{NH4/NO3}}*({}^{18}\mathrm{F}_{\mathrm{O2}}/{}^{18}\alpha_{\mathrm{AMO(O2)}} + {}^{18}\mathrm{F}_{\mathrm{H2O}}/{}^{18}\alpha_{\mathrm{AMO(H2O)}}) + R_{\mathrm{NH4/NO3}}*{}^{18}\mathrm{F}_{\mathrm{H2O}}/{}^{18}\alpha_{\mathrm{NXR(H2O)}}$$
$$- 3*R_{\mathrm{NO3comp}}/{}^{18}\alpha_{\mathrm{NO3comp}}*{}^{18}\mathrm{F}_{\mathrm{NO3}}$$

Table S4. Parameters used in the isotopologue-specific model for simulating net mineralization, nitrification, and nitrate consumption.

Parameter	Description	Value	Comment
$[^{14}N]$, $[^{15}N]$, $[^{16}O]$, $[^{17}O]$, $[^{18}O]$	N or O isotopologue concentration		Simulated by the model
^{14}F, ^{15}F	Fractional abundance of ^{14}N or ^{15}N		Calculated from isotopologue concentrations
^{16}F, ^{17}F, ^{18}F	Fractional abundance of ^{16}O, ^{17}O, or ^{18}O		Calculated from isotopologue concentrations
$R_{OrgN/NH4}$	Zero order rate for net mineralization		Optimized by the model
$R_{NH4/NO3}$	Zero order rate for gross nitrification		Optimized by the model
$R_{NO3comp}$	Zero order rate for gross NO_3^- consumption		Optimized by the model
$^{15}\alpha_{OrgN/NH4}$	N fractionation factor for net mineralization		Optimized by the model
$^{15}\alpha_{NH4/NO3}$	N fractionation factor for gross nitrification		Optimized by the model
$^{15}\alpha_{NO3comp}$	N fractionation factor for gross NO_3^- consumption		Optimized by the model
$^{18}\alpha_{NO3comp}$	O fractionation factor for H_2O incorporation during NXR-catalyzed NO_2^- oxidation		Set to be coupled to $^{15}\alpha_{NO3comp}$ for each model iteration
$^{18}\alpha_{AMO(O2)}$	O fractionation factor for O_2 incorporation by aerobic NH_3 oxidation	1.014	Casciotti et al. (2010); Granger and Wankel (2016)
$^{18}\alpha_{AMO(H2O)}$	O fractionation factor for H_2O incorporation by aerobic NH_3 oxidation	1.014	Casciotti et al. (2010); Granger and Wankel (2016)
$^{18}\alpha_{NXR(H2O)}$	O fractionation factor for H_2O incorporation during NXR-catalyzed NO_2^- oxidation	1.014	Buchwald and Casciotti, (2010)

S6. Data tables of the anoxic, oxic, hypoxic, and abiotic incubation experiments.

Table S5. NO_3^- and NO_2^- concentrations and net NO production rates during the anoxic incubation.

Sampling time (h)	NO_3^- ($\mu g\ N \cdot g^{-1}$)	NO_2^- ($\mu g\ N \cdot g^{-1}$)	$f_{NO\text{-}anoxic}$ ($ng\ N \cdot g^{-1} \cdot h^{-1}$)
0.0	49.3±0.1	0.4±0.1	71.8±8.2
25.3	44.7±0.1	1.2±0.3	73.8±2.2
48.3	41.2±0.6	1.9±0.2	72.6±3.1
73.8	37.8±0.3	2.8±0.2	75.6±2.1
97.6	32.6±0.6	4.2±0.3	81.9±3.1
121.6	29.2±0.9	5.2±0.4	79.5±0.2
145.0	26.2±0.9	5.4±0.6	81.5±1.4
169.1	23.1±0.2	6.9±0.1	81.3±0.3

Table S6. Isotopic composition of NO_3^-, NO_2^-, and NO during the anoxic incubation.

Sampling time (h)	$\delta^{15}N\text{-}NO_3^-$ (‰)	$\delta^{18}O\text{-}NO_3^-$ (‰)	$\Delta^{17}O\text{-}NO_3^-$ (‰)	$\delta^{15}N\text{-}NO_2^-$ (‰)[a]	$\delta^{15}N\text{-}NO$ (‰)
0.0	4.7±0.3	33.4±0.2	10.0±0.2	NA	-44.7±0.3[b]
25.3	8.7±0.2	33.0±0.4	8.4±0.5	NA	-43.5±0.7
48.3	12.8±0.2	31.4±0.9	6.0±0.3	NA	-40.2±1.2
73.8	17.4±0.8	28.7±0.3	4.5±0.4	NA	-37.1±0.9
97.6	22.6±0.6	26.8±0.3	2.9±0.2	NA	-32.8±1.2
121.6	26.7±0.7	26.1±0.9	1.6±0.2	-6.9±3.7	-29.1±0.4
145.0	31.0±1.2	24.5±1.3	1.1±0.6	-6.0±2.5	-26.8±0.3
169.1	38.7±1.5	23.1±0.3	0.7±0.1	0.9±1.3	-20.8±2.2[b]

a: NA: not measured due to low NO_2^- concentrations.

b: mean and standard deviation were calculated based on two replicates.

Table S7. NO_3^- and NH_4^+ concentrations and net NO production rates during the oxic incubation.

Sampling time (h)	NH_4^+ (μg N·g^{-1})	NO_3^- (μg N·g^{-1})	$f_{\text{NO-oxic}}$ (ng N·g^{-1}·h^{-1})[a]
Low δ^{15}N-NH_4^+			
0.0	87.2±3.3	46.8±0.6	NA
26.2	73.0±1.5	55.8±1.1	8.0±0.1
50.5	63.7±1.2	65.5±0.1	7.7±0.2
76.8	54.2±1.6	76.2±0.4	7.4±0.1
Intermediate δ^{15}N-NH_4^+			
0.0	88.9±0.7	45.3±0.2	NA
26.4	74.8±0.8	55.2±0.2	8.2±0.0
50.3	64.5±1.4	65.0±0.1	7.9±0.1
74.4	53.7±1.0	75.4±0.3	7.1±0.1
High δ^{15}N-NH_4^+			
0.0	86.5±1.0	45.7±0.1	NA
26.3	74.1±0.9	54.9±0.5	8.5±0.1
50.3	64.4±0.2	65.1±0.7	8.0±0.1
74.4	54.7±0.7	75.0±0.4	7.5±0.1

a: NA: no measurement.

Table S8. Isotopic composition of NO_3^-, NH_4^+, and NO during the oxic incubation.

Sampling time (h)	δ^{15}N-NH_4^+ (‰)	δ^{15}N-NO_3^- (‰)	δ^{18}O-NO_3^- (‰)	Δ^{17}O-NO_3^- (‰)	δ^{15}N-NO (‰)[a]
Low δ^{15}N-NH_4^+					
0.0	-0.5±0.2	2.6±0.1	19.2±0.2	6.9±0.1	NA
26.2	4.0±1.6	-3.2±0.4	15.0±0.4	5.3±0.1	-54.9±0.8
50.5	7.4±2.5	-6.3±0.0	11.8±0.0	4.3±0.1	-53.3±0.5
76.8	11.4±0.2	-8.3±0.0	9.8±0.5	3.8±0.3	NA
Intermediate δ^{15}N-NH_4^+					
0.0	22.6±2.2	2.7±0.3	20.0±0.2	7.0±0.2	NA
26.4	24.1±1.0	1.2±0.1	15.5±0.2	5.3±0.1	-37.4±1.3
50.3	29.7±1.3	0.8±0.5	12.3±0.4	4.2±0.1	-33.5±0.2
74.4	31.2±2.1	1.6±0.6	10.7±0.4	3.8±0.1	NA
High δ^{15}N-NH_4^+					
0.0	43.3±2.1	2.8±0.3	18.9±0.2	6.9±0.1	NA
26.3	50.8±2.3	5.2±0.8	14.6±1.0	5.4±0.0	-17.9±1.9[b]
50.3	53.9±3.4	8.0±0.1	11.7±0.6	4.4±0.1	-16.8±0.3
74.4	56.4±3.4	10.6±0.3	9.6±0.3	3.9±0.4	NA

a: NA: no measurement.

b: mean and standard deviation were calculated based on two replicates.

Table S9. NO_3^- and NH_4^+ concentrations and NO production rates during the hypoxic incubation.

Sampling time (h)	NH_4^+ ($\mu g\ N \cdot g^{-1}$)	NO_3^- ($\mu g\ N \cdot g^{-1}$)	$f_{NO\text{-hypoxic}}$ ($\mu g\ N \cdot g^{-1} \cdot h^{-1}$)[a]
Low $\delta^{15}N$-NH_4^+			
0.0	89.6±0.9	46.2±0.2	NA
26.2	87.5±0.4	47.0±0.1	10.0±0. 0
50.5	86.0±0.4	48.3±0.1	9.8±0. 1
76.8	84.3±0.3	49.1±0.6	9.4±0.2
Intermediate $\delta^{15}N$-NH_4^+			
0.0	89.1±1.6	46.5±0.1	NA
26.4	87.0±2.2	47.5±0.2	10.4±0.2
50.3	85.1±1.8	48.7±0.1	9.6±0.1
74.4	83.1±0.1	49.7±0.0	9.0±0.1
High $\delta^{15}N$-NH_4^+			
0.0	89.9±0.8	46.0±0.1	NA
26.3	87.8±0.4	46.9±0.3	10.4±0.1
50.3	86.0±0.8	48.3±0.2	10.0±0.1
74.4	82.1±1.1	49.1±0.3	9.5±0.2

a: NA: no measurement.

Table S10. Isotopic composition of NO_3^-, NH_4^+, and NO during the hypoxic incubation.

Sampling time (h)	$\delta^{15}N$-NH_4^+ (‰)	$\delta^{15}N$-NO_3^- (‰)	$\delta^{18}O$-NO_3^- (‰)	$\Delta^{17}O$-NO_3^- (‰)	$\delta^{15}N$-NO (‰)[a]
Low $\delta^{15}N$-NH_4^+					
0.0	-0.7±1.4	2.6±0.2	19.2±0.2	7.0±0.1	NA
26.2	-0.2±0.5	1.0±0.1	17.4±0.2	6.6±0.1	-50.5±1.0
50.5	-1.0±0.9	0.3±0.2	16.5±0.0	6.4±0.2	-51.4±0.4
76.8	-0.2±4.2	-0.4±0.1	15.9±0.2	5.8±0.2	NA
Intermediate $\delta^{15}N$-NH_4^+					
0.0	20.9±1.6	2.8±0.1	19.3±0.1	6.8±0.1	NA
26.4	21.3±2.9	2.4±0.2	17.0±0.4	6.4±0.2	-38.5±0.2
50.3	21.8±0.4	2.7±0.3	16.3±0.4	6.0±0.2	-37.2±0.2
74.4	22.6±0.8	3.6±0.1	15.6±0.1	5.6±0.2	NA
High $\delta^{15}N$-NH_4^+					
0.0	45.1±1.5	3.1±0.2	19.2±0.1	6.7±0.1	NA
26.3	45.2±2.5	4.1±0.1	16.9±0.3	6.2±0.1	-24.3±1.7
50.3	45.2±3.2	5.2±0.2	16.1±0.1	6.0±0.1	-21.3±0.0[b]
74.4	47.1±3.0	6.9±0.1	15.2±0.1	5.4±0.2	NA

a: NA: no measurement.

b: mean and standard deviation were calculated based on two replicates.

Table S11. Rate and isotopic composition of abiotic NO production in the NO_2^--amended sterile soil under anoxic conditions.

Time (h)	$f_{NO\text{-}abiotic}$ (ng N·g^{-1}·h^{-1})	δ^{15}N-NO (‰)[a]
0.4	82.5±4.6	-17.8±0.4
20.9	55.2±3.1	NA
48.7	30.9±2.9	NA
74.6	18.1±1.5	NA
91.6	12.4±1.2	NA
120.9	7.9±0.9	NA
145.1	4.7±0.5	NA
170.1	3.5±0.3	NA
189.4	2.6±0.2	NA

a: NA: no measurement.

S7. Supplementary figures.
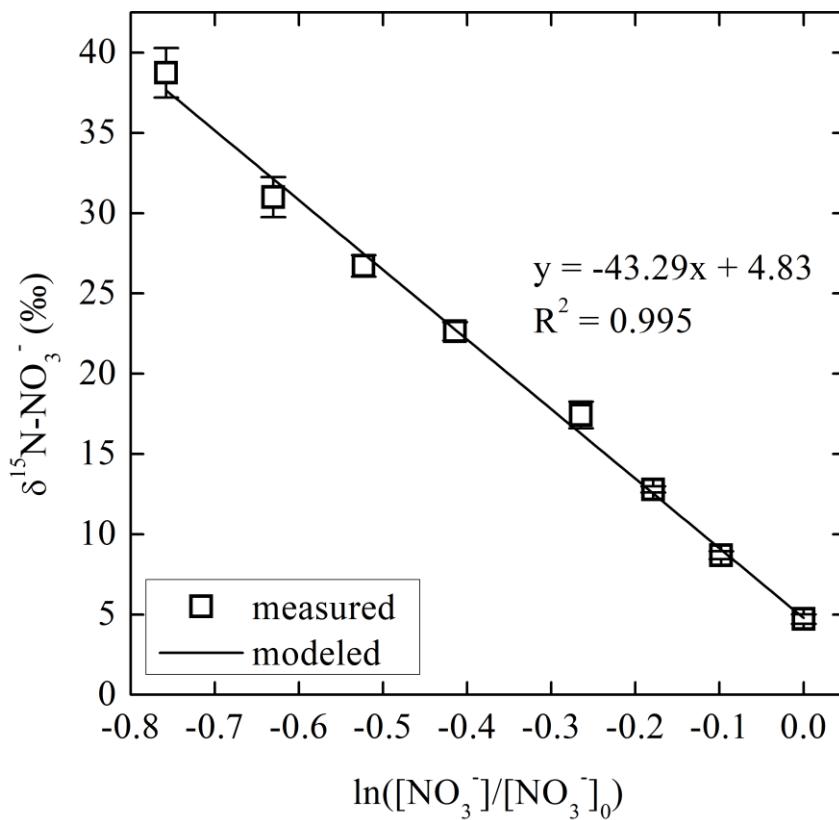
Figure S3. Rayleigh plot of $\delta^{15}N\text{-}NO_3^-$ versus the natural logarithm of factional NO_3^- consumption. The slope of linear regression gives an estimate of the apparent N isotope effect for NO_3^- consumption during the anoxic incubation.
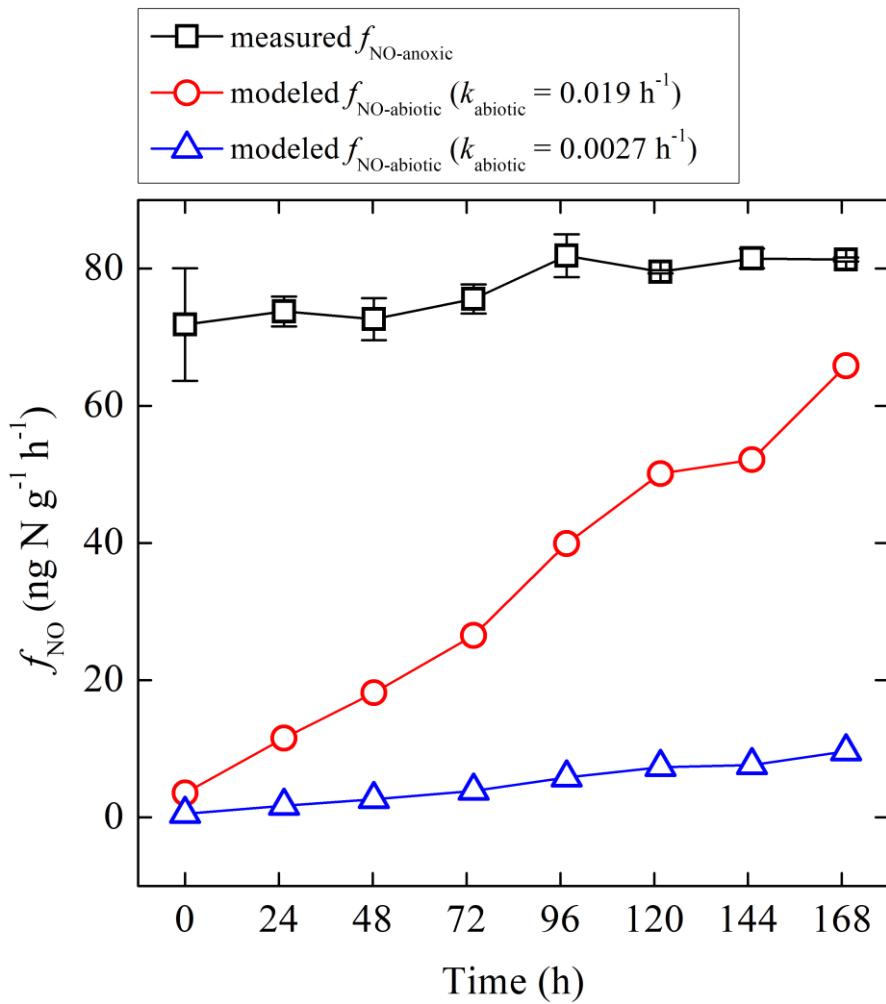
Figure S4. Comparison between the measured net NO production rates during the anoxic incubation, modeled abiotic NO production rates using $k_{abiotic}$ derived in the abiotic incubation, and modeled abiotic NO production rates using a reduced $k_{abiotic}$.

S8. References:

Buchwald C. and Casciotti K. L.: Oxygen isotopic fractionation and exchange during bacterial nitrite oxidation, Limnol. Oceanogr., 55, 1064-1074, 2010.

Casciotti K. L., McIlvin M. and Buchwald C.: Oxygen isotopic exchange and fractionation during bacterial ammonia oxidation, Limnol. Oceanogr., 55, 753-762, 2010.

Casciotti K. L., Sigman D. M., Hastings M. G., Böhlke J. K. and Hilkert A.: Measurement of the oxygen isotopic composition of nitrate in seawater and freshwater using the denitrifier method, Anal. Chem., 74, 4905-4912, 2002.

Fry B.: Stable isotope ecology (Vol. 521), New York: Springer, 2006.

Granger J. and Wankel S. D.: Isotopic overprinting of nitrification on denitrification as a ubiquitous and unifying feature of environmental nitrogen cycling, Proc. Natl. Acad. Sci. U.S.A., 113, E6391-E6400, 2016.

Lewicka-Szczebak D., Well R., Köster J. R., Fuß R., Senbayram M., Dittert K. and Flessa H.: Experimental determinations of isotopic fractionation factors associated with N_2O production and reduction during denitrification in soils, Geochim. Cosmochim. Acta, 134, 55-73, 2014.

Miller M. F.: Isotopic fractionation and the quantification of ^{17}O anomalies in the oxygen three-isotope system: an appraisal and geochemical significance, Geochim. Cosmochim. Acta, 66, 1881-1889, 2002.

Taylor A. E., Taylor K., Tennigkeit B., Palatinszky M., Stieglmeier M., Myrold D. D., Schleper C., Wagner M. and Bottomley P. J.: Inhibitory effects of C_2 to C_{10} 1-alkynes on ammonia oxidation in two Nitrososphaera species, Appl. Environ. Microbiol., 81, 1942-1948, 2015.

Young E. D., Galy A., Nagahara H.: Kinetic and equilibrium mass-dependent isotope fractionation laws in nature and their geochemical and cosmochemical significance, Geochim. Cosmochim. Acta, 66, 1095-1104, 2002.

Yu Z. and Elliott E. M.: Probing soil nitrification and nitrate consumption using $\Delta^{17}O$ of soil nitrate, Soil Biol. Biochem., 127, 187-199, 2018.